Inorg. Chem. **2008**, *47*, 9478−9488

Supramolecular Luminescent Gold(I)−Copper(I) Complexes: Self-Assembly of the Au_xCu_y Clusters inside the $[Au_3(diphosphine)_3]^{3+}$ Triangles

Igor O. Koshevoy,*,† Antti J. Karttunen,† Sergey P. Tunik,*,‡ Matti Haukka,† Stanislav I. Selivanov,‡ Alexei S. Melnikov,§ Pavel Yu. Serdobintsev,§ Mikhail A. Khodorkovskiy,§ and Tapani A. Pakkanen*,†

Department of Chemistry, University of Joensuu, 80101, Joensuu, Finland, Department of Chemistry, St.-Petersburg State University, Universitetskii pr. 26, 198504, St.-Petersburg, Russia, Department of Physics, St.-Petersburg State University, Ulijanovskaja 3, 198504, St. Petersburg, Russia

Received June 11, 2008

The reactions between diphosphino−alkynyl gold complexes $(PhC_2Au)PPh_2(C_6H_4)_nPPh_2(AuC_2Ph)$ ($n = 1, 2, 3$) with Cu^+ lead to formation of the heterometallic aggregates, the composition of which may be described by a general formula $[\{Au_xCu_y(C_2Ph)_{2x}\}Au_3\{PPh_2(C_6H_4)_nPPh_2\}_3]^{3+(y-x)}$ ($n = 1, 2, 3$; $x = (n + 1)(n + 2)/2$; $y = n(n + 1)$). These compounds display very similar structural patterns and consist of the $[Au_xCu_y(C_2Ph)_{2x}]^{y-x}$ alkynyl clusters "wrapped" in the $[Au_3(diphosphine)_3]^{3+}$ triangles. The complex for $n = 1$ was characterized crystallographically and spectrally, the larger ones ($n = 2, 3$) were investigated in detail by NMR spectroscopy. Their luminescence behavior has been studied, and a remarkably efficient emission with a maximum quantum yield of 0.92 ($n = 1$) has been detected. Photophysical experiments demonstrate that an increase of the size of the aggregates leads to a decrease in photostability and photoefficiency. Computational studies have been performed to provide additional insight into the structural and electronic properties of these supramolecular complexes. The theoretical results obtained are in good agreement with the experimental data, supporting the proposed structural motif. These studies also suggest that the observed efficient long-wavelength luminescence originates from metal-centered transitions within the heterometallic Au−Cu core.

Introduction

Chemistry of the polynuclear d^{10} alkynyl complexes continues to be an area of intense research and has significantly progressed during the past decade. The rich structural diversity of these compounds and their attractive physical properties, such as optical nonlinearity, luminescence, and liquid crystallinity,[1−5] serve as a driving force behind the recent advances. Through the combination of metallophilic interaction and the σ or π bonding mode of the alkyne ligands, which are able to bridge multiple metal centers, numerous polynuclear species have been successfully prepared and investigated. The structures of these cluster compounds, particularly of those containing phosphine ligands, are often complicated,[4,6−14] and in many cases, the

* Authors to whom correspondence should be addressed. E-mail: igor.koshevoy@joensuu.fi (I.O.K.), tapani.pakkanen@joensuu.fi (T.A.P.), stunik@inbox.ru (S.P.T.).
† University of Joensuu.
‡ Department of Chemistry, St.-Petersburg State University.
§ Department of Physics, St.-Petersburg State University.

(1) Long, N. J.; Williams, C. K. *Angew. Chem., Int. Ed.* **2003**, *42*, 2586–2617.
(2) Lang, H.; George, D. S. A.; Rheinwald, G. *Coord. Chem. Rev.* **2000**, *206−207*, 101–197.
(3) Yam, V. W.-W. *Acc. Chem. Res.* **2002**, *35*, 555–563.
(4) Yip, S.-K.; Cheng, E. C.-C.; Yuan, L.-H.; Zhu, N.; Yam, V. W.-W. *Angew. Chem., Int. Ed.* **2004**, *43*, 4954–4957.
(5) Powell, C. E.; Humphrey, M. G. *Coord. Chem. Rev.* **2004**, *248*, 725–756.
(6) Rais, D.; Yau, J.; Mingos, D. M. P.; Vilar, R.; White, A. J. P.; Williams, D. J. *Angew. Chem., Int. Ed.* **2001**, *40*, 3464–3467.
(7) de la Riva, H.; Nieuwhuyzen, M.; Fierro, C. M.; Raithby, P. R.; Male, L.; Lagunas, M. C. *Inorg. Chem.* **2006**, *45*, 1418–1420.
(8) Wei, Q.-H.; Zhang, L.-Y.; Yin, G.-Q.; Shi, L.-X.; Chen, Z.-N. *J. Am. Chem. Soc.* **2004**, *126*, 9940–9941.
(9) Wei, Q.-H.; Yin, G.-Q.; Zhang, L.-Y.; Shi, L.-X.; Mao, Z.-W.; Chen, Z.-N. *Inorg. Chem.* **2004**, *43*, 3484–3491.
(10) Wei, Q.-H.; Yin, G.-Q.; Zhang, L.-Y.; Chen, Z.-N. *Organometallics* **2005**, *25*, 4941–4944.
(11) Wei, Q.-H.; Zhang, L.-Y.; Yin, G.-Q.; Shi, L.-X.; Chen, Z.-N. *Organometallics* **2005**, *24*, 3818–3820.
(12) Yin, G.-Q.; Wei, Q.-H.; Zhang, L.-Y.; Chen, Z.-N. *Organometallics* **2006**, *25*, 580–587.

10.1021/ic801073k CCC: $40.75
Published on Web 09/19/2008

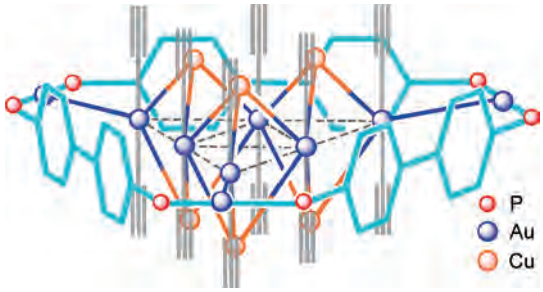

Figure 1. Schematic structure of trication $[\{Au_6Cu_6(C_2Ph)_{12}\}Au_3(PPh_2(C_6H_4)_2PPh_2)_3]^{3+}$ (**1**). Phenyl rings omitted for clarity.

assembly of the complexes occurs in an uncontrolled way and leads to unpredictable products. Their emissive properties are strongly influenced by the presence of metallophilic (in particular, aurophilic) interactions and the possible changes of the electron-donating characteristics of the alkyne ligands via π coordination to encapsulated metal ions.[7,13,15−17] Therefore, it is a challenging and fascinating task to search for the synthetic routes, which would not only lead to novel organometallic compounds with unusual molecular topologies and unique physical properties but also allow for the feasible modification of the structural and electronic features of these complexes.

In our recent publication,[14] we presented the reactions of a relatively simple di-gold complex based on a rigid diphosphine ligand with the Cu^+ cation to give a self-assembled supramolecular gold−copper cluster (Figure 1), which contains the central $[Au_6Cu_6(C_2Ph)_{12}]$ fragment, wrapped about by the $[AuPPh_2(C_6H_4)_2PPh_2]_3^{3+}$ "belt" anchored to the central part by the Au−Au bonds. The reaction proceeds through rearrangement of the ligands' environment but does not involve any oxidation−reduction process, thus retaining a formal oxidation state of the Au and Cu ions of +1 as in the starting materials.

It was also possible to perform the assembly of this complex in a stepwise manner via independent synthesis of its constituents—the central part $[Au_6Cu_6(C_2Ph)_{12}]$ and the external "belt" $[AuPPh_2(C_6H_4)_2PPh_2]_2^{2+}$ (in the form of a dimer)—and their subsequent coupling into the title compound. The heterometallic compounds obtained display a bright long-wavelength luminescence from an excited state of triplet origin in contrast to well-known alkynyl−phosphine complexes of gold,[18,19] which normally emit in the blue region of the spectrum with a relatively low quantum yield of luminescence.[20−24] These changes in photophysical properties of the gold-containing complexes are evidently due to the coordination of Cu^+ ions to PhC_2-Au-C_2Ph fragments, thus modifying the electronic structure of the HOMO−LUMO block through interaction with $\pi^*(C\equiv C)$ and d(Au) orbitals. These observations prompted us to further explore this chemistry, searching for a possible general synthetic strategy and accessible limits of the size variations of the molecules and to get deeper insight into the photophysical and electronic features of this type of compound. Thus, our intention was to prepare a series of structurally related Au−Cu heterometallic compounds using the diphosphine ligands with various lengths of oligophenylene spacer between P atoms, to study their luminescence behavior and to perform theoretical calculations of the electronic structures of the complexes to correlate their structural and photophysical properties.

Experimental Section

General Comments. (Au(tht)Cl (tht = tetrahydrothiophene),[25] $(AuC_2Ph)_n$,[26] 1,4-bis(diphenylphosphino)benzene,[27] 4,4″-dibromoterphenyl,[28] and $[\{Au_6Cu_6(C_2Ph)_{12}\}Au_3(PPh_2(C_6H_4)_2PPh_2)_3][PF_6]_3$[14] (**1**) were synthesized according to published procedures. Tetrahydrofuran was distilled over Na-benzophenoneketyl under a nitrogen atmosphere prior to use. The synthesis of 4,4″bis(diphenylphosphino)-terphenyl was carried out under a nitrogen atmosphere. Other reagents and solvents were used as received. Solution ^1H, ^{13}C, and ^{31}P NMR spectra were recorded on Bruker Avance 400 and Bruker DPX 300 spectrometers. The 2D COSY and phase-sensitive NOESY spectra were run using standard Bruker pulse sequences. Mass spectra were determined on a Bruker APEX-Qe ESI FT-ICR instrument, in the ESI^+ mode. Microanalyses were carried out in the analytical laboratory of St.-Petersburg State University. UV−vis spectra were recorded on a Shimadzu UV 3600 spectrophotometer.

1,4-$(PhC_2AuPPh_2)_2C_6H_4$ (2). Complex **2** was obtained by a slight modification of a reported procedure.[29] $(AuC_2Ph)_n$ (100 mg, 0.336 mmol) was suspended in CH_2Cl_2 (10 cm^3). 1,4′-Bis(diphenylphosphino)benzene (77 mg, 0.173 mmol) was added, and the yellow suspension turned into a colorless transparent solution within minutes. It was diluted with toluene (10 cm^3) and stirred for 30 min in the absence of light. The resulting solution was passed through Al_2O_3 (0.5 × 2 cm, neutral, ∼150 mesh) and concentrated to ca. 5 cm^3. A white microcrystalline solid was precipitated by centrifugation, washed with toluene (5 cm^3) and diethyl ether (2 × 5 cm^3), and vaccuum-dried. Yield: 162 mg (93%). $^{31}P\{^1H\}$ NMR ($CDCl_3$; δ): 41.7 (s). ^1H NMR ($CDCl_3$; δ): 7.65−7.47 (m, 28H), 7.29−7.14 (m, 6H).

(13) Tang, H.-S.; Zhu, N.; Yam, V. W.-W. *Organometallics* **2007**, *26*, 22–25.
(14) Koshevoy, I. O.; Koskinen, L.; Haukka, M.; Tunik, S. P.; Serdobintsev, P. Y.; Melnikov, A. S.; Pakkanen, T. A. *Angew. Chem., Int. Ed.* **2008**, *47*, 3942–3945.
(15) Charmant, J. P. H.; Fornies, J.; Gomez, J.; Lalinde, E.; Merino, R. I.; Moreno, M. T.; Orpen, A. G. *Organometallics* **1999**, *18*, 3353–3358.
(16) Yam, V. W.-W.; Cheung, K.-L.; Cheng, E. C.-C.; Zhu, N.; Cheung, K.-K. *Dalton Trans.* **2003**, 1830–1835.
(17) Vicente, J.; Chicote, M.-T.; Alvarez-Falcon, M. M.; Jones, P. G. *Organometallics* **2005**, *24*, 4666–4675.
(18) Yam, V. W.-W.; Lo, K. K.-W.; Wong, K. M.-C. *J. Organomet. Chem.* **1999**, *578*, 3–30.
(19) Yam, V. W.-W.; Cheung, K.-L.; Yip, S.-K.; Cheung, K.-K. *J. Organomet. Chem.* **2003**, *681*, 196–209.
(20) Liu, L.; Wong, W.-Y.; Shi, J.-X.; Cheah, K.-W.; Lee, T.-H.; Leung, L. M. *J. Organomet. Chem.* **2006**, *691*, 4028–4041.
(21) Liu, L.; Wong, W.-Y.; Poon, S.-Y.; Shi, J.-X.; Cheah, K.-W.; Lin, Z. *Chem. Mater.* **2006**, *18*, 1369–1378.
(22) Heng, W. Y.; Hu, J.; Yip, J. H. K. *Organometallics* **2007**, *26*, 6760–6768.
(23) Lu, W.; Zhu, N.; Che, C.-M. *J. Organomet. Chem.* **2003**, *670*, 11–16.
(24) Poon, S.-Y.; Wong, W.-Y.; Cheah, K.-W.; Shi, J.-X. *Chem.—Eur. J.* **2006**, *12*, 2550–2563.
(25) Uson, R.; Laguna, A.; Laguna, M. *Inorg. Synth.* **1989**, *26*, 85–91.
(26) Coates, G. E.; Parkin, C. *J. Chem. Soc.* **1962**, 3220–3226.
(27) Baldwin, R. A.; Cheng, M. T. *J. Org. Chem.* **1967**, *32*, 1572–1577.
(28) Wang, Z.; Heising, J. M.; Clearfield, A. *J. Am. Chem. Soc.* **2003**, *125*, 10375–10383.
(29) Yam, V. W.-W.; Choi, S. W.-K.; Cheung, K.-K. *Organometallics* **1996**, *15*, 1734–1739.

[{Au$_3$Cu$_2$(C$_2$Ph)$_6$}Au$_3$(PPh$_2$C$_6$H$_4$PPh$_2$)$_3$][PF$_6$]$_2$ (3). Complex **2** (120 mg, 0.115 mmol) was dissolved in CH_2Cl_2 (10 cm^3) and diluted with diethyl ether (5 cm^3), and a solution of Cu(NCMe)$_4$PF$_6$ (28 mg, 0.075 mmol) in CH_2Cl_2 (5 cm^3) was added dropwise. A bright yellow-orange solution was stirred for 30 min in the absence of light. Solvents were removed on a rotary. A yellow-orange solid was recrystallized by the gas-phase diffusion of pentane into its acetone solution at 5 °C to give orange plate crystals (119 mg, 87%). ES MS (*m*/*z*): [Au$_6$Cu$_2$(C$_2$Ph)$_6$(PPh$_2$C$_6$H$_4$PPh$_2$)$_3$]$^{2+}$, 1627 (calcd 1627). ^{31}P{^{1}H} NMR (acetone-d$_6$; δ): 43.6 (s, 3P), −144.8 (sept, 1P, PF$_6$). ^{1}H NMR (acetone-d$_6$; δ), **{Au(C$_2$Ph)$_2$}**: 6.75 (dd, H-ortho, 12H, *J*(H−H) 8.2, 1.3 Hz), 6.83 (dd, H-meta, 12H, *J*(H−H) 7.5, 8.2 Hz), 7.13 (tt, H-para, 6H, *J*(H−H) 7.5, 1.3 Hz). **Diphosphine**: 7.98 (dm(AXX′), H-ortho, 24H, *J*(H−H) 8.2, *J*(P−H) 13.4 Hz), 7.76 (m(A$_2$X$_2$), {P−C$_6$H$_4$−P} 12H, <*J*(P−H)> 3.6 Hz), 7.65 (t, H-para, 12H, *J*(H−H) 7.5 Hz), 7.45 (dm(AXX′), H-meta, 24H, *J*(H−H) 8.2, 7.5 Hz). ^{13}C NMR (acetone-d$_6$; δ), **{Au(C$_2$Ph)$_2$}**: 133.76 and 129.87 (s, C-ortho and C-meta), 129.47 (s, C-para), 125.33 (s, C-ipso), 114.54 (s, C≡C−Au), 112.69 (s, C≡C−Au). **Diphosphine**: 137.37 (m (AXX′), C (−C$_6$H$_4$−), *J*(P−C) 58.8 Hz), 137.04 (m (AXX′), C-ortho, *J*(P−C) 16.5 Hz), 135.64 (m (AXX′), C(H) (−C$_6$H$_4$−), *J*(P−C) ca. 11 Hz), 134.61 (s, C-para), 131.70 (s, C-meta), 129.84 (m (AXX′), C-ipso, *J*(P−C) 55.5 Hz). Anal. calcd for C$_{138}$H$_{102}$Au$_6$Cu$_2$F$_{12}$P$_8$: C, 46.76; H, 2.90. Found: C, 46.92; H, 3.30.

4,4″-Bis(diphenylphosphino)-terphenyl (4). 4,4″-Dibromoterphenyl (1 g, 2.6 mmol) was suspended in THF (60 cm^3); the suspension was cooled to −70 °C, and a 1.6 M solution of *n*-BuLi in hexanes (4.5 mL, 7.2 mmol) was added within 5 min. The reaction mixture was slowly (ca. 4 h) warmed to −10 °C, stirred at this temperature for 1 h more, and then cooled again to −70 °C, and neat PPh$_2$Cl (1.55 g, 7.0 mmol) was added dropwise. The cooling bath was removed; the reaction mixture was allowed to reach room temperature and was stirred overnight. Then, it was filtered; volatiles were evaporated, and an oily yellow residue was thoroughly washed with methanol (4 × 30 cm^3) to give a white solid that was recrystallized from $CHCl_3$/methanol (1.0 g, 65%). ES MS (*m*/*z*): [*M*$^+$] 598 (calcd 598). ^{31}P{^{1}H} NMR ($CDCl_3$; δ): −5.6 (s). ^{1}H NMR ($CDCl_3$; δ): 7.68 (s, 4H, −C$_6$H$_4$−), 7.62 (dd, *J*(H−H) 8.2, *J*(P−H) 1.5 Hz, 4H, −C$_6$H$_4$−P), 7.41 (dd, *J*(H−H) 8.2, *J*(P−H) 7.5 Hz, 4H, −C$_6$H$_4$−P), 7.39−7.36 (m, 20H, Ph$_2$P). Anal. calcd for C$_{42}$H$_{32}$P$_2$: C, 84.26; H, 5.39. Found: C, 83.98; H, 5.34.

4,4″-(PhC$_2$AuPPh$_2$)$_2$(C$_6$H$_4$)$_3$ (5). (AuC$_2$Ph)$_n$ (110 mg, 0.369 mmol) was suspended in CH_2Cl_2 (10 cm^3). Complex **4** (115 mg, 0.192 mmol) was added, and the yellow suspension turned into a colorless transparent solution within minutes. It was diluted with toluene (10 cm^3) and stirred for 30 min in the absence of light. The resulting solution was passed through Al_2O_3 (0.5 × 2 cm, neutral, ∼150 mesh) and concentrated to ca. 5 cm^3. A white microcrystalline solid was precipitated by centrifugation, washed with toluene (5 cm^3) and diethyl ether (2 × 5 cm^3), and vaccuum-dried. Yield: 205 mg (93%). An analytically pure sample was obtained by recrystallization from CH_2Cl_2/toluene. ^{31}P{^{1}H} NMR ($CDCl_3$; δ): 41.3 (s). ^{1}H NMR ($CDCl_3$; δ): 7.74−7.46 (m, 36H), 7.30−7.15 (m, 6H). ^{13}C{^{1}H} NMR ($CDCl_3$; δ), **diphosphine**: 143.37 (d, C(−C$_6$H$_4$−), *J*(P−C) 2.4 Hz), 139.24 (d, para-C(−C$_6$H$_4$−P), *J*(P−C) 1.3 Hz), 134.74 (d, ortho-C(−C$_6$H$_4$−P), *J*(P−C) 14.1 Hz), 134.17 (d, ortho-C(Ph−P), *J*(P−C) 13.9 Hz), 131.55 (d, para-C(Ph−P), *J*(P−C) 2.4 Hz), 129.58 (d, ipso-C(Ph−P), *J*(P−C) 56.1 Hz), 129.10 (d, meta-C(Ph−P), *J*(P−C) 11.4 Hz), 128.57 (d, ipso-C(−C$_6$H$_4$−P), *J*(P−C) 56.5 Hz), 127.73 (s, CH(−C$_6$H$_4$−)), 127.51 (d, meta-C(−C$_6$H$_4$−P), *J*(P−C) 11.6 Hz). **{Au(C$_2$Ph)}**: 132.22 (s, ortho-C (Ph−C≡C)), 127.84 (s, meta-C (Ph−C≡C)), 126.70 (s, para-C (Ph−C≡C)), 124.76 (s, ipso-C (Ph−C≡C)), ca. 104.1 (br (Ph−C≡C)). Anal. calcd for C$_{58}$H$_{42}$Au$_2$P$_2$: C, 58.30; H, 3.54. Found: C, 58.14; H, 3.74.

[{Cu$_{12}$Au$_{10}$(C$_2$Ph)$_{20}$}Au$_3$(PPh$_2$(C$_6$H$_4$)$_3$PPh$_2$)$_3$][PF$_6$]$_5$ (6). Complex **5** (200 mg, 0.168 mmol) was dissolved in CH_2Cl_2 (10 cm^3), and a solution of Cu(NCMe)$_4$PF$_6$ (41 mg, 0.201 mmol) in acetone (6 cm^3) was added dropwise. A bright red-orange solution was stirred for 30 min in the absence of light and diluted with heptane (5 cm^3), and solvents were removed on a rotary evaporator. A red residue was extracted with an acetone/heptane mixture (3:1 v/v, 4 × 8 cm^3) to leave a pale insoluble material. Solvents were evaporated, and extraction was repeated with the same solvent mixture. Subsequent recrystallization from a CH_2Cl_2 solution at 5 °C by gas-phase diffusion of the pentane gave red crystals and a nearly colorless solid, the majority of which was mechanically removed. The product, **6**, was extracted with an acetone/heptane mixture (3:1 v/v, 4 × 8 cm^3) to leave some pale insoluble material. Solvents were evaporated to give a red microcrystalline powder. Final recrystallization under the conditions mentioned above gave a red crystalline solid (95 mg, 47% based on Au). ^{31}P{^{1}H} NMR (acetone-d$_6$; δ): 42.8 (s, 6P), −144.8 (sept, 5P, PF$_6$). ^{1}H NMR (acetone-d$_6$; δ), **diphosphine**: 8.47 (s, −C$_6$H$_4$−, 12H), 8.375 (d, meta-H, (−C$_6$H$_4$−P), 12H, *J*(H−H) 8.3 Hz), 7.80 (dm (AXX′), ortho-H, (−C$_6$H$_4$−P), 12H, *J*(H−H) 8.3, *J*(P−H) 6.3 Hz), 7.66 (dm (AXX′), ortho-H, (Ph−P), 24H, *J*(H−H) 8.4, *J*(P−H) 6.8 Hz), 7.60 (t, para-H, (Ph−P), 12H, *J*(H−H) 7.5 Hz), 7.34 (dd, meta-H, (Ph−P), 24H, *J*(H−H) 8.4, 7.5 Hz). **{Au(C$_2$Ph)$_2$} rods** (three set of rods **A/B/C = 1:3:6** for numbering scheme, see text), **A**: 7.30 (d, ortho-H, 4H, *J*(P−H) 8.1 Hz), 7.21 (t, para-H, 2H, *J*(P−H) 7.7 Hz), 6.19 (dd, meta-H, 4H, *J*(P−H) 7.7, 8.1 Hz). **B**: 7.19 (t, para-H, 6H, *J*(P−H) 7.5 Hz), 6.81 (dd, meta-H, 12H, *J*(P−H) 7.5, 8.1 Hz), 6.23 (d, ortho-H, 12H, *J*(P−H) 8.1 Hz). **C**: 7.11 (t, para-H, 12H, *J*(P−H) 7.6 Hz), 6.85 (d, ortho-H, 24H, *J*(P−H) 8.3 Hz), 6.64 (dd, meta-H, 24H, *J*(P−H) 7.6, 8.3 Hz). ^{13}C NMR (acetone-d$_6$; δ), **diphosphine**: 144.53 (s, para-C (P−C$_6$H$_4$)), 140.73 (s, C (−C$_6$H$_4$−)), 136.73 (m (AXX′), ortho-C, (P−C$_6$H$_4$), *J*(P−C) 14.4 Hz), 136.53 (m (AXX′), ortho-C, (P−Ph), *J*(P−C) 15.6 Hz), 134.5 (s, para-C, (P−Ph)), 131.57 (m (AXX′), meta-C, (P−C$_6$H$_4$), *J*(P−C) 11.8 Hz), 130.26 (s, CH (−C$_6$H$_4$−)), 129.73 (m (AXX′), ipso-C, (P−Ph), *J*(P−C) 57.6 Hz), 129.68 (m (AXX′), meta-C, (P−C$_6$H$_4$), *J*(P−C) 11.0 Hz), 129.67 (m (AXX′), ipso-C, (P−C$_6$H$_4$), *J*(P−C) 59.5 Hz). **{Au(C$_2$Ph)$_2$} rods** (three set of rods **A/B/C = 1:3:6** for numbering scheme see text), **A**: 135.92 (s, ortho-C), 133.80 (s, para-C), 131.01 (s, meta-C), 120.67 (s, ipso-C), 120.03 (s, C≡C−Au), 98.70 (s, C≡C−Au). **B**: 134.44 (s, ortho-C), 130.68 (s, para-C), 130.03 (s, meta-C), 123.46 (s, ipso-C), 120.72 (s, C≡C−Au), 107.53 (s, C≡C−Au). **C**: 134.97 (s, ortho-C), 132.38 (s, para-C), 130.38 (s, meta-C), 124.94 (s, C≡C−Au), 121.40 (s, ipso-C), 101.50 (s, C≡C−Au). Anal. calcd for C$_{286}$H$_{196}$Au$_{13}$Cu$_{12}$F$_{30}$P$_{11}$: C, 43.67; H, 2.51. Found: C, 43.69; H, 2.68.

Photophysical Measurements. An Excimer laser, LPX 100 (Lambda Physik), and light-emitting diode (LED; maximum emission at 470 nm) were used to pump luminescence. The laser pulse width was 35 ns; pulse energy, 160 mJ; and repetition rate, 1−25 Hz. A LED was used in the continue and pulse mode (pulse width, 1−20 μs; duty of edge, ∼90 ns; repetition rate, 100 Hz to 10 kHz). A digital oscilloscope, Tektronix TDS3014B (Tektronix, bandwidth 100 MHz), and photodiode with a 10 ns time resolution were used for lifetime measurements. Emission spectra were recorded using an HR2000 spectrometer (Ocean Optics). A halogen lamp, LS-1-CAL (Ocean Optics), and deuterium lamp, DH2000 (Ocean Optics), were used to calibrate the absolute spectral response

Scheme 1

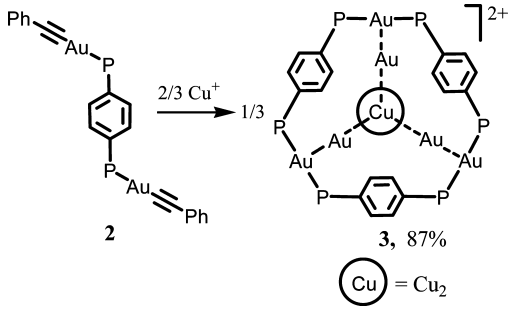

of the spectral system in the 200−875 nm range. All solutions were carefully degassed before lifetime measurements. Lifetime measurements were done using laser (308nm) and LED (maximum emission at 470 nm) pumping; monoexponential decay was observed for all compounds studied. The absolute emission quantum yield was determined by Vavilov's method (optically dense solution modification)[30] using LED (470 nm, continue mode) pumping and rhodamine 6G (Φ_{em}=0.95 ± 0.03) as a standard.

X-Ray Crystal Structure Determinations. The crystals were immersed in cryo-oil, mounted in a Nylon loop, and measured at a temperature of 120 K. The X-ray diffraction data were collected by means of a Nonius KappaCCD diffractometer using Mo Kα radiation (λ = 0.71073 Å). *EvalCCD*[31] program packages was used for cell refinements and data reductions. The structure was solved by direct methods using the *SHELXS-97*[32] program with the *WinGX*[33] graphical user interface. An empirical absorption correction was applied to all of the data (*SADABS*).[34] Structural refinements were carried out using *SHELXH-97*.[35] One of the acetone solvent molecules was partially lost from the structure. Therefore, it was refined with an occupancy of 0.5. Another acetone molecule was disordered over two sites with occupancies of 0.57/0.43. Carbon atoms C103, C104, C146, C147, C148, C149, C150, C151, and C152 (in acetone molecules or aromatic rings) were restrained so that their U_{ij} components approximated to isotropic behavior. All hydrogen atoms were positioned geometrically and constrained to ride on their parent atoms, with C−H = 0.95−0.98 Å and U_{iso} = 1.2−1.5 U_{eq} (parent atom). The crystallographic details are summarized in Table S1 (S denotes Supporting Information).

Computational Details. The studied systems were fully optimized without any symmetry constraints using the BP86 density functional method.[36−38] Because the van der Waals type aurophilic Au−Au interactions are not properly described by DFT methods,[39,40] spin-component-scaled[41] MP2 (SCS-MP2) single-point energy calculations were performed at the BP86 optimized geometries. The electron-correlated MP2 method accounts for the aurophilic interactions,[40] and the SCS-MP2 method has been shown to decrease the overbinding effect of the ordinary MP2.[41] The copper and gold atoms were described with a triple-valence ζ-quality basis set with polarization functions (def2-TZVP),[42] employing a 60-electron relativistic effective core potential for gold.[43] A split-valence basis set with polarization functions on non-hydrogen atoms was used for all of the other atoms (def2-SV(P)).[44] The resolution-of-the-identity technique was used to speed up both DFT[45−48] and SCS-MP2[49−51] calculations. Natural population analyses[52] were performed at the BP86 level of theory. All of the calculations were carried out with TURBOMOLE versions 5.9.1 and 5.10.[53]

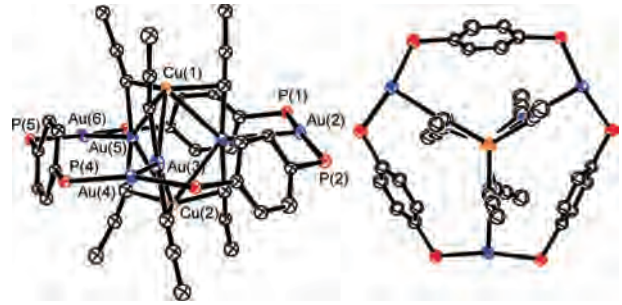

Figure 2. Two ORTEP projections of the dication **3**. Phenyl rings and hydrogen atoms omitted for clarity. Selected interatomic distances (Å) are Au(1)−Au(2) = 2.8649(6), Au(3)−Au(4) = 2.8730(7), Au(5)−Au(6) = 2.8665(8), Au(1)−Cu(1) = 2.8516(13), Au(1)−Cu(2) = 2.9088(13), Au(3)−Cu(1) = 2.8923(13), Au(3)−Cu(2) = 2.8324(13), Au(5)−Cu(1) = 2.7572(12), Au(5)−Cu(2) = 2.8768(13).

Results and Discussion

Synthesis and Characterization. The reaction of the digold complex $[Au_2(C{\equiv}CPh)_2(\mu\text{-}1,4\text{-}PPh_2C_6H_4PPh_2)]$ (**2**) with a stoichiometric amount of $[Cu(NCMe)_4PF_6]$ in dichloromethane leads to formation of the novel cluster compound $[\{Au_3Cu_2(C_2Ph)_6\}Au_3(PPh_2C_6H_4PPh_2)_3][PF_6]_2$ (**3**) in good yield (Scheme 1).

Bright-orange air-stable complex **3** has been characterized by ^{1}H, ^{13}C, and ^{31}P NMR and ESI-MS spectrometry. Its structure in the solid state has been determined by X-ray diffraction analysis. An ORTEP view of the dication **3** is shown in Figure 2. The ESI mass spectrum of **3** (Figure S1) displays a signal of a doubly charged cation at *m*/*z* 1627, the isotopic pattern of which completely fits the stoichiometry of the $[\{Au_3Cu_2(C_2Ph)_6\}Au_3(PPh_2C_6H_4PPh_2)_3]^{2+}$ molecular ion.

(30) Demas, J. N.; Crosby, G. A. *J. Phys. Chem.* **1971**, *75*, 991–1024.
(31) Duisenberg, A. J. M.; Kroon-Batenburg, L. M. J.; Schreurs, A. M. M. *J. Appl. Crystallogr.* **2003**, *36*, 220–229.
(32) Sheldrick, G. M. *SHELXS97*; University of Gottingen: Gottingen, Germany, 1997.
(33) Farrugia, L. J. *J. Appl. Crystallogr.* **1999**, *32*, 837–838.
(34) Sheldrick, G. M. *SADABS*, 2.10; Bruker Analytical X-ray Systems, Bruker Axs Inc.: Madison, WI, 2003.
(35) Sheldrick, G. M. *SHELXH-97*; University of Gottingen: Gottingen, Germany, 1997.
(36) Becke, A. D. *Phys. Rev. A: At., Mol., Opt. Phys.* **1988**, 3098–3100.
(37) Vosko, S. H.; Wilk, L.; Nusair, M .*Can. J. Phys* **1980**, *58*, 1200–1211.
(38) Perdew, J. P. *Phys. Rev. B: Condens. Matter Mater. Phys.* **1986**, *33*, 8822–8824.
(39) Scherbaum, F.; Grohmann, A.; Huber, B.; Krüger, C.; Schmidbaur, H. *Angew. Chem., Int. Ed.* **1988**, *27*, 1544–1546.
(40) Pyykko, P. *Angew. Chem., Int. Ed.* **2004**, *43*, 4412–4456.
(41) Grimme, S. *J. Chem. Phys.* **2003**, *118*, 9095–9102.
(42) Weigend, F.; Ahlrichs, R. *Phys. Chem. Chem. Phys.* **2005**, *7*, 3297–3305.
(43) Andrae, D.; Häuβermann, U.; Dolg, M.; Stoll, H.; Preuβ, H. *Theor. Chem. Acc.* **1990**, *77*, 123–141.
(44) Schäfer, A.; Horn, H.; Ahlrichs, R. *J. Chem. Phys.* **1992**, *97*, 2571–2577.
(45) Eichkorn, K.; Treutler, O.; Öhm, H.; Häser, M.; Ahlrichs, R. *Chem. Phys. Lett.* **1995**, *240*, 283–290.
(46) Sierka, M.; Hogekamp, A.; Ahlrichs, R. *J. Chem. Phys.* **2003**, *118*, 9136–9148.
(47) Eichkorn, K.; Weigend, F.; Treutler, O.; Ahlrichs, R. *Theor. Chem. Acc.* **1997**, *97*, 119–124.
(48) Weigend, F. *Phys. Chem. Chem. Phys.* **2006**, *8*, 1057–1065.
(49) Weigend, F.; Häser, M. *Theor. Chem. Acc.* **1997**, *97*, 331–340.
(50) Hättig, C.; Weigend, F. *J. Chem. Phys.* **2000**, *113*, 5154–5161.
(51) Weigend, F.; Häser, M.; Patzelt, H.; Ahlrichs, R. *Chem. Phys. Lett.* **1998**, *294*, 143–152.
(52) Reed, A. E.; Weinstock, R. B.; Weinhold, F. *J. Chem. Phys.* **1985**, *83*, 735–746.
(53) Ahlrichs, R.; Bär, M.; Häser, M.; Horn, H.; Kölmel, C. *Chem. Phys. Lett.* **1989**, *62*, 165–169.

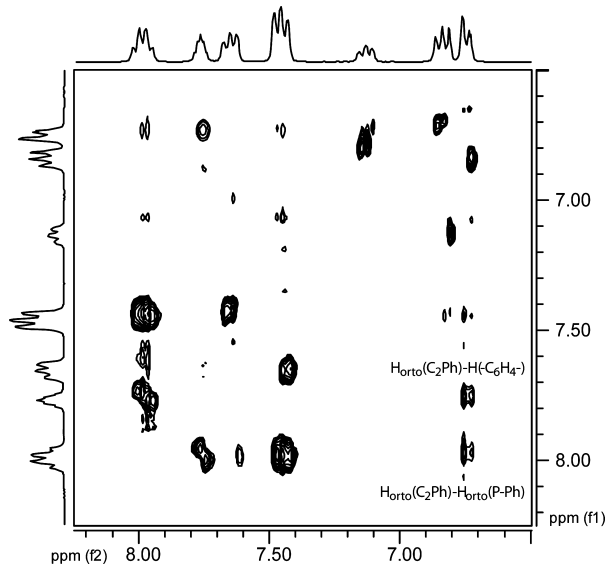

Figure 3. Negative part of the NOESY spectrum of **3** (τ_{mixing} 0.6 s), 300 MHz, acetone-d_6, 298 K. Crosspeaks generated by adjacent protons of a phenyl ring are not marked in the figure. Antiphase diagonal signals are not shown.

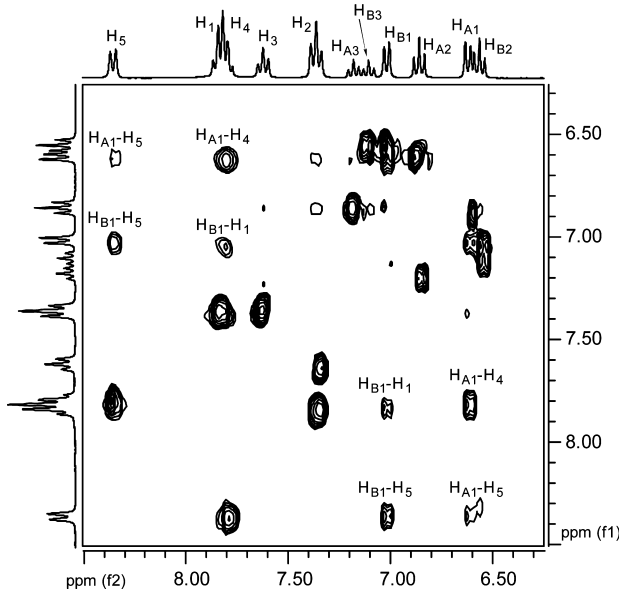

Figure 4. Negative part of the NOESY spectrum of cluster **1** (τ_{mixing} 0.6 s), 300 MHz, acetone-d_6, 298 K. Crosspeaks generated by adjacent protons of a phenyl ring are not marked in the figure. Antiphase diagonal signals are not shown. For numbering scheme, see Chart 1.

The molecule contains the central $[Au_3Cu_2(C_2Ph)_6]$ fragment, which is wrapped about by the $[AuPPh_2(C_6H_4)_2PPh_2]_3$ "belt" anchored to the central part by the Au−Au bonds. The Au−Au contacts of 2.8649(6), 2.8730(7), and 2.8665(8) Å fall in the range of values typical for aurophilic interaction.[4,8,40,54,55] The Au−P bond lengths in the $[AuPPh_2C_6H_4PPh_2]_3$ triangle lie in the range from 2.301(2) to 2.321(2) Å (average 2.309 Å), which is in accord with the previously reported values for linear gold phosphine cationic complexes.[56−59] The central fragment consists of three approximately parallel $[PhC_2AuC_2Ph]$ rods held together by Cu−Au, π−C≡C−Cu, and, to a lesser extent, weak Au−Au bonding. The metal atoms form a trigonal bipyramid with two copper atoms in the apical positions, each of which being π-bonded to three alkynyl groups. Three gold atoms occupy the equatorial sites of the bipyramid; the equatorial plane is slightly tilted (6.7 °) with respect to the plane of the external $[AuPPh_2C_6H_4PPh_2]_3$ "belt". The Au···Au distances within the Au_3Cu_2 cluster vary from 3.3347(9) to 3.3603(7) Å, which is indicative of quite weak aurophilic interaction. The Cu−Au contacts are significantly shorter and were found to be between 2.7572(12) and 2.9088(13) Å (average 2.853 Å). These values are substantially lower than the sum of the Au and Cu van der Waals radii (3.06 Å) and lie within the range found for the other gold−copper complexes (2.6−3.0 Å) with direct Au−Cu bonding.[7,60,61] It should be noted that the $[Au_3Cu_2(C_2Ph)_6]^-$ anion has been reported previously,[60] and has the same geometry as the central part of **3**. However, the metal−metal distances in **3** are slightly shorter than those in $[Au_3Cu_2(C_2Ph)_6]^-$. It is worth noting that self-assembling of the molecule driven by Cu−Au, Au−Au, and π−C≡C−Cu bonding brings together organic fragments of the alkynyl and diphosphine ligands, which display short nonbonding contacts both in the solid state and in solution. In particular, the contacts of ortho-protons of the alkynyl ligands with adjacent protons of the C_6H_4 spacer according to X-ray data range from 2.54 to 3.18 Å (av = 2.83 ± 0.30 Å) that in turn afford NOE connectivities linking the corresponding protons in the negative part of the NOESY spectrum, see below.

The NMR data obtained for **3** are completely consistent with the structure described above. The ^{31}P NMR spectrum displays a resonance at 43.6 ppm that corresponds to the equivalent phosphorus atoms of the diphosphine ligands, in addition to the $[PF_6]^-$ septuplet at −144 ppm. The signals observed in the ^1H NMR spectrum of **3** can be interpreted on the basis of the $^1H-^1H$ COSY spectrum, Figure S2, and coupling to the phosphorus nuclei. The high-field (7.12 ppm, t, 1H; 6.83 ppm, d, 2H; 6.75 ppm, dd, 2H) set of resonances, which does not display coupling to phosphorus, is assigned to para/ortho/meta protons of the $[PhC_2AuC_2Ph]$ moieties. Correlations observed in the low-field part of the COSY spectrum (8.0 − 7.4 ppm) allow assignment of this group of signals to the phenyl rings (7.98 ppm, ortho-H; 7.65 ppm, para-H; 7.45 ppm, meta-H) and the C_6H_4 spacer (7.76 ppm) of the diphosphine ligand. Clearly visible coupling of the ortho-phenyl protons (dm, J(P−H) 13.4 Hz and protons of the C_6H_4 spacer (A_2X_2 spin system, $<J(P-H)>$ 3.6 Hz) to the phosphorus nuclei support the suggested assignment. The

(54) Pyykko, P. *Chem. Rev.* **1997**, *97*, 597–636.
(55) Fernandez, E. J.; Gimeno, M. C.; Laguna, A.; Lopez-de-Luzuriaga, J. M.; Monge, M.; Pyykko, P.; Sundholm, D. *J. Am. Chem. Soc.* **2000**, *122*, 7287–7293.
(56) Fu, W.-F.; Chan, K.-C.; Cheung, K.-K.; Che, C.-M. *Chem.—Eur. J.* **2001**, *7*, 4656–4664.
(57) Heuer, B.; Pope, S. J. A.; Reid, G. *Polyhedron* **2000**, *19*, 743–749.
(58) Slawin, A. M. Z.; Smith, M. B.; Woollins, J. D. *Polyhedron* **1999**, *18*, 1135–1140.
(59) Bella, P. A.; Crespo, O.; Fernández, E. J.; Fischer, A. K.; Jones, P. G.; Laguna, A.; López-de-Luzuriaga, J. M.; Monge, M. *J. Chem. Soc., Dalton Trans.* **1999**, 4009–4017.
(60) Abu-Salah, O. M.; Al-Ohaly, A. R. A.; Knobler, C. B. *J. Chem. Soc., Chem. Commun.* **1985**, 1502–1503.
(61) Hao, L.; Mansour, M. A.; Lachicotte, R. J.; Gysling, H. J.; Eisenberg, R. *Inorg. Chem.* **2000**, *39*, 5520–5529.

Scheme 2

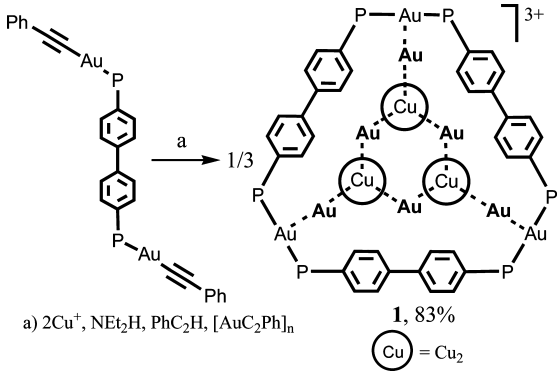

Chart 1

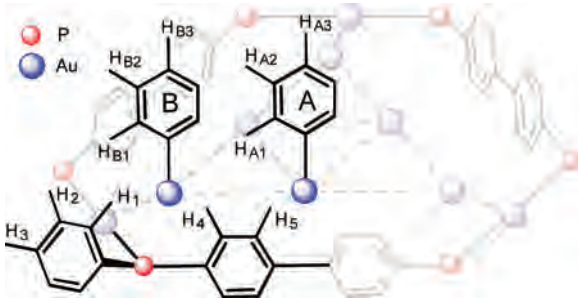

^{13}C NMR spectroscopic data (see the Experimental Section) are also consistent with the structure revealed in the solid state. Detailed assignment of the proton NMR spectrum makes it possible to use the NOESY data (Figure 3) in the interpretation of the molecular structure in solution. In addition to the regular connectivities generated by the short contacts of the adjacent aromatic protons, clearly visible crosspeaks between the ortho-protons of the [PhC_2AuC_2Ph] moieties and the protons of the diphosphine spacer are indicative of rigidity of the molecular structure based on rather weak aurophilic interactions retaining alkynyl "rods" inside the diphosphine "belt".

The reaction of the closest relative of **2**, complex [Au_2(C≡CPh)$_2$(μ-4,4′-$PPh_2(C_6H_4)_2PPh_2$)], based on a diphosphine with a biphenyl spacer between phosphorus atoms, with stoichiometric amounts of [$Cu(MeCN)_4$][PF_6], [AuC≡CPh]$_n$, and PhC≡CH in the presence of NEt_2H leads to formation of the previously reported complex [{$Au_6Cu_6(C_2Ph)_{12}$}-$Au_3(PPh_2(C_6H_4)_2PPh_2)_3$][$PF_6$]$_3$ (**1**; Scheme 2, Figure 1).[14]

The composition and structure of this complex were established on the basis of its ^{1}H, ^{13}C, and ^{31}P NMR and ESI-MS data and were confirmed by X-ray crystallography. The structural relation to complex **3** is clearly visible—expansion of the diphosphine ligand's length leads to an increase of the internal space inside the triangular [Au_3(diphosphine)$_3$] "belt" and subsequent growth of the "wrapped" cluster [Au_xCu_y]—from [$Au_3Cu_2(C_2Ph)_6$] in **3** to [$Au_6Cu_6(C_2Ph)_{12}$]. The inner [Au_6Cu_6] cluster consists of two groups of the [PhC_2AuC_2Ph] rods, which form large and small triangles, and are evidently structurally inequivalent (Chart 1).

The rods are held together by the Au−Cu and Au−Au bonding interactions, which are strong enough to make the structure rigid in solution. The signals of the alkynyl phenyl rings in both the ^{1}H and ^{13}C NMR spectra are clearly segregated to give two sets of multiplets of equal intensity; see, for example, the 1D projection in Figure 4. The NOESY spectrum (Figure 4) displays crosspeaks between the ortho protons of the alkynyl phenyls and the protons of the biphenyl spacer, very similar to those detected in the NOESY spectrum of **3**. This observation is a clear indication of the cluster skeleton rigidity and structural similarity of these compounds.

As a natural extension of the synthetic results described above, we explored the chemistry of a terphenyl-based diphosphine $PPh_2(C_6H_4)_3PPh_2$ (**4**). The treatment of gold phenylacetylide [AuC≡CPh]$_n$ with this ligand leads to clean formation of the complex [Au_2(C≡CPh)$_2$(μ-4,4″-PPh_2-$(C_6H_4)_3PPh_2$)] (**5**) with the longest spatial separation between two metal centers among the compounds under study, which was completely characterized ^{1}H,^{13}C, and ^{31}P NMR spectroscopy and elemental analysis. The addition of [Cu(MeCN)$_4$][PF_6] in acetone to a colorless solution of **5** in dichloromethane immediately turns its color to orange-red. Workup of the reaction mixture afforded a deep-red complex [{$Au_{10}Cu_{12}(C_2Ph)_{20}$}$Au_3(PPh_2(C_6H_4)_3PPh_2)_3$][$PF_6$]$_5$ (**6**). Colorless material, obtained as a side product, can be formulated as a dinuclear compound [$AuPPh_2(C_6H_4)_3PPh_2]_2^{2+}$ according to the data of its ESI MS spectroscopic analysis (Figure S3). An analogous complex, [$AuPPh_2(C_6H_4)_2PPh_2]_2^{2+}$, has been obtained as a side-product in the course of formation of **1**[14] (Scheme 3).

Complex **6** did not give crystals suitable for X-ray analysis, and its composition and the structure have been established on the basis of its elemental analysis and a detailed

Scheme 3

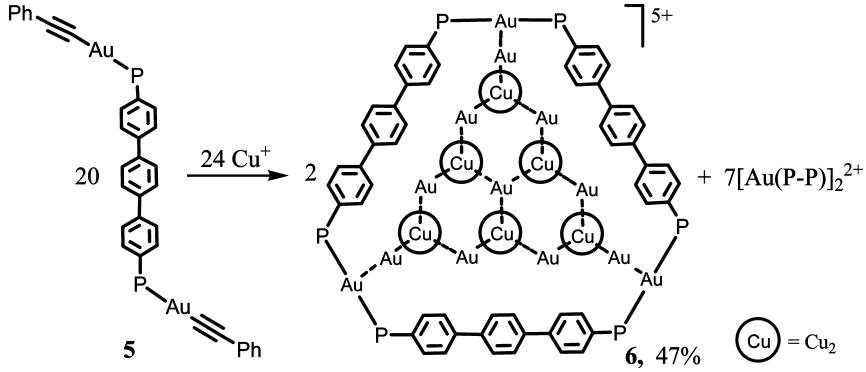

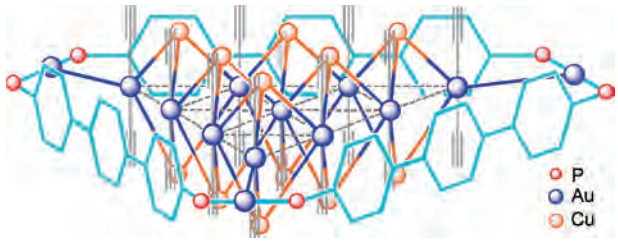

Figure 5. Schematic structure of pentacation **6**. Phenyl rings omitted for clarity.

investigation of the ^{1}H, ^{13}C, and ^{31}P NMR spectroscopic data together with a comparative analysis of the spectroscopic parameters obtained for clusters **3** and **1**. Similarity of the chemistry observed in the reactions of the $[Au_2(C{\equiv}CPh)_2(\mu\text{-}PPh_2(C_6H_4)_nPPh_2)]$ ($n = 1-3$) complexes with Cu^+ indicates that the mechanism of self-assembling of the gold−copper aggregates is essentially analogous in all of these cases, and the structural patterns of the final products are based on closely related topologies. Provided that the "rods-in-belt" motif is also operative for product **6**, its schematic structure may be depicted as shown in Figure 5.

The molecule evidently contains the $[Au_3(PPh_2(C_6H_4)_3\text{-}PPh_2)_3]^{3+}$ "belt" with an encapsulated array of dialkynyl−gold "rods" held together by Cu^+ ions. To keep the D_{3h} symmetry of the central fragment (as in the cases of smaller congeners), expansion of the array should result in the formation of a planar decanuclear Au_{10} core with 12 (six above and six below) copper ions, each of which is coordinated to three alkynyl triple bonds and three gold centers. The formal charge of the central fragment amounts to +2 to give, in total, +5 for the whole molecule. Therefore, the composition of this series of "rods-in-belt" complexes may be described by a general formula $[\{Au_xCu_y(C_2Ph)_{2x}\}Au_3\{PPh_2-(C_6H_4)_n-PPh_2\}_3]^{3+(y-x)}$ ($n = 1, 2, 3$; $x = (n + 1)(n + 2)/2$; $y = n(n + 1)$).

The NMR spectroscopic data strongly support this structural hypothesis. The ^{31}P NMR spectrum displays one signal at 42.8 ppm that fits completely the D_{3h} symmetry group of the molecule. Analysis of the correlations in the $^{1}H-^{1}H$ COSY spectrum (Figure S4) shows that the signals observed in the low-field region (8.50−7.31 ppm, Figure 6) belong to the protons of the diphosphine ligands, relative intensities of this group of signals being completely consistent with this assignment. This segregation of the signals corresponding to the diphosphine ligand and alkynyl−gold rods is also typical for the low nuclear congeners of **6**: complexes **3** and **1**.[14]

In addition to typical proton−proton couplings, the signals

Chart 2

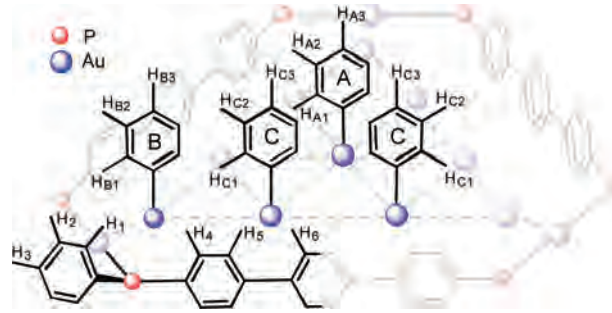

of the protons adjacent to the phosphorus atoms display $^{31}P-^{1}H$ spin−spin coupling constants in accord with their stereochemical disposition. The correlations observed in the high-field part of the COSY spectrum split the proton signals into three groups with characteristic relative intensities 1:3:6, each of which has a typical phenyl moiety multiplicity (2:2:1 = ortho(d)/meta(dd)/para(t)). This observation is completely consistent with the D_{3h} symmetry of the $(PhC_2AuC_2Ph)_{10}$ core, where a unique central rod (**A**) is encircled by nine neighbors, three of which seat in the corners of the triangle (**B**), whereas six others (**C**) occupy the positions on the sides of the triangle, thus forming three groups of structurally different rods—**A**, **B**, and **C**, respectively (Chart 2).

Analysis of the ^{13}C (Experimental Section), DEPT, and HSQC (Figure S5) NMR spectra revealed similar discrimination of the signals, which are divided into three groups with the relative intensity 1:3:6, which is also completely consistent with the structural hypothesis suggested for **6**. Another important argument in favor of the "rods-in-belt" structure was found in the NOE NMR spectrum (Figure 7).

The cross-peaks observed in the negative part of the spectrum relate to the ortho-protons of the **C** (H_{C1}) and **A** (H_{A1}) rods; the former are also related to the protons of the central phenylene spacer of the diphosphine (H_6) and adjacent protons (H_4, H_5) of the $P-C_6H_4$ fragment. This points to the short nonbonding contacts between these protons that are completely consistent with the disposition of these rods in the central core as well as with the proximity of ortho protons of the **C** group to the central part of the terphenylene spacer. In turn, ortho protons of **B** rods (H_{B1}) located in the corners of the Au_{10} triangle display correlations with the ortho protons of $P-C_6H_4-$ (H_4) and P−Ph (H_1) moieties of the diphosphine, pointing to their spatial proximity dictated by the mutual disposition of these fragments in the molecule. These observations are also in line

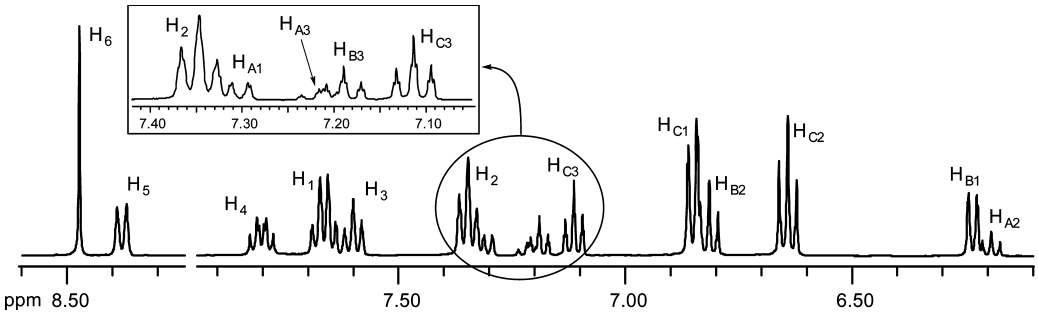

Figure 6. The ^{1}H NMR spectrum of **6**, 400 MHz, acetone-d_6, 298 K. Assignment of the signals corresponds to the numbering scheme given in Chart 2.

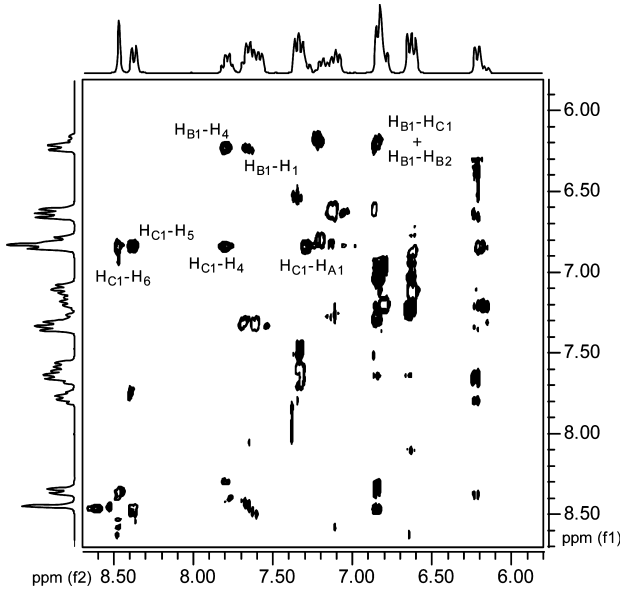

Figure 7. Negative part of the NOESY spectrum of **6** (τ_{mixing} 0.6 s), 300 MHz, acetone-d_6, 298 K. Crosspeaks generated by adjacent protons of a phenyl ring are not marked in the figure. Antiphase diagonal signals are not shown. For the numbering scheme, see Chart 2.

with the correlations observed in the NOE spectrum of **3**, where analogous groups of protons generate crosspeaks, the origin of which is strongly supported by the corresponding short nonbonding contacts found in the solid-state structure of this complex. Thus, the combination of various NMR techniques allows for unambiguous structural characterization of the supramolecular aggregate **6**.

Photophysical Characteristics of Supramolecular Au−Cu Aggregates. Spectroscopic data for the complexes **1**, **3**, **5**, and **6** are given in Table 1. Complex **5** displays absorption bands between 230 and 300 nm typical of the alkynyl−phosphine complexes[62] and its smaller congeners.[14,29] The high-energy absorption below 250 nm is normally assigned to intraligand transitions, whereas the band centered at 300 nm can be assigned to the promotion of an electron from the σ(Au−P) orbital to an empty π^* antibonding orbital located at the bridging phenyl group.[29,62] The heterometallic complexes containing the [Au_xCu_y] cluster core in addition to the absorption in the ultraviolet region display broad bands located at ca. 400 nm. Because neither alkynyl−phosphine complexes nor dialkynyl−gold anionic compounds[63] display visible area absorption, the orbitals of the heterometallic framework are evidently involved in the transitions responsible for these low-energy bands; see also, the computational results given below.

All of the compounds shown in Table 1 are luminescent

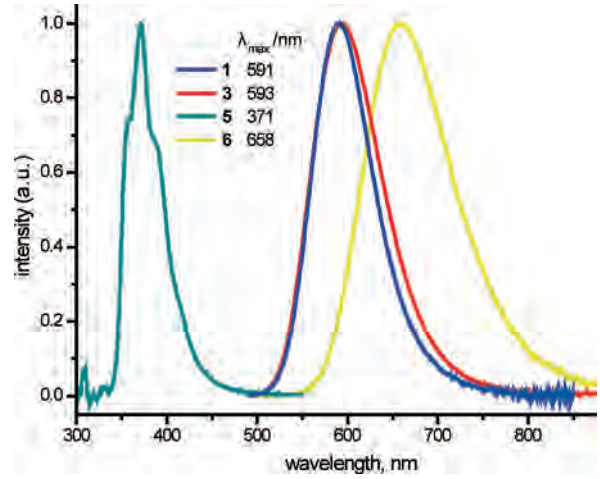

Figure 8. Room-temperature normalized emission spectra of **1**, **3**, **5**, and **6** using CH_2Cl_2, λ_{excit} = 308 nm.

(Figure 8), but the emitting properties of **5** are essentially different from those found for the complexes containing a [Au_xCu_y] heterometallic core. Homonuclear complex **5** under 308 nm laser excitation displays a poorly structured emission band centered at 371 nm, similar to analogous digold complexes studied earlier.[14,29] The lifetime of this emitting excited state is shorter than 30 ns, which points to its singlet origin.

All three heterometallic clusters are much stronger luminophors to give emission bands with the maxima 593, 591, and 658 nm, Table 1. It has to be noted that emission parameters (λ_{max}, band half-width, τ) do not depend on the excitation wavelengths, which were varied (308, 470, 520, and 530 nm) using a few light sources. The lifetime of these excited states ranges from 5.5 to 9.5 μs, which clearly points to their triplet origin. This is an indication of effective intersystem crossing into an emitting triplet state independent of the nature of initial excited state. The most striking feature of the heterometallic clusters' luminescence is unprecedented emission quantum yield. Typical quantum yield values for homometallic alkynyl−(phosphine, pyridine) gold complexes are of a few percent only,[63,64] and very few polyalkynyl compounds show good quantum efficiency (up to 0.52).[21,65] The unprecedented effective luminescence of **3** is comparable with the quantum yield of a typical dye laser working medium, like for example rhodamine 6G, which opens a potential way to use the compounds of this sort in lasing applications.

Computational Results. Quantum chemical calculations were performed to provide additional insight into the structural and electronic properties of the supramolecular Au(I)−Cu(I) complexes (for computational details, see the

Table 1. Spectroscopic data for **1**, **3**, and **5**, at 298 K, CH_2Cl_2

complex	λ_{ab}/nm, (10^{-3} ε/dm^3 mol^{-1} cm^{-1})	λ_{em}/nm[a]	τ/μs[b]	Φ_{em}[c]
1	286 (219.6), 398 (58.3)	591	9.5 ± 0.1[d]	0.6 ± 0.1
3	262 (179), 403 (34.3)	593	5.5 ± 0.1	0.92 ± 0.08
5[e]	246 sh (32.4), 272 sh (28.5), 285 sh (39.5), 296 (42.6)	371	<30 ns	<0.01
6	293 (280), 307 sh (265), 408 (74.8)	658	7.6 ± 0.1	0.46 ± 0.08

[a] λ_{excit} = 470 nm. [b] The data obtained under λ_{excit} = 308, 470 nm. [c] λ_{excit} = 470 nm. Steady-state regime, relative to rhodamine 6G (Φ_{em} = 0.95 ± 0.03). [d] This value is slightly different from the value given in ref14 because of the use of dichloromethane distilled immediately prior to use. This solvent evidently accumulates an extremely effective luminescence quencher after being kept for a few days. The luminescence spectrum is not sensitive to this factor. [e] λ_{excit} = 308 nm.

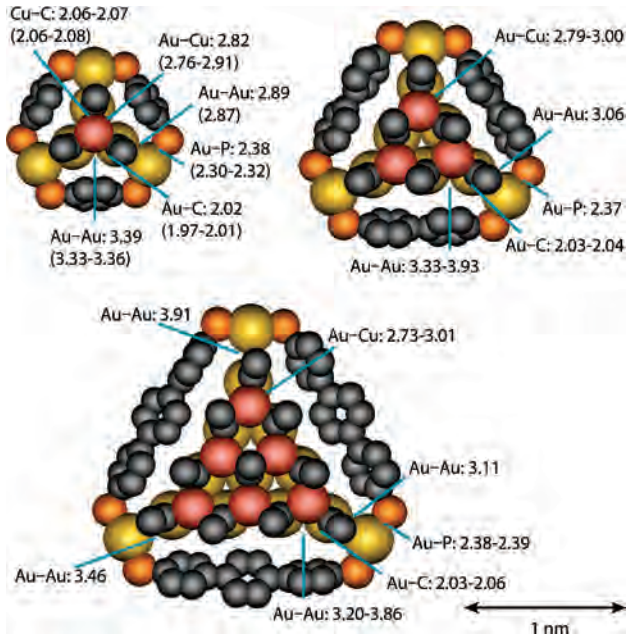

Figure 9. Optimized geometries and selected structural parameters for dication **3** (top left), trication **1** (top right), and pentacation **6** (bottom). For **3**, the experimental structural parameters are listed in parentheses. The complexes are shown from a top view, omitting phenyl rings and hydrogen atoms for clarity.

Experimental Section). The optimized geometries and selected structural parameters of all three studied "rods-in-belt" complexes, obtained using the BP86 density functional (DFT) method, are shown in Figure 9. For the smallest complex, **3**, it was possible to compare the DFT-optimized geometry to the X-ray crystal structure, and the comparison between the theoretical and experimental structural parameters shows them to be in good agreement. Geometry optimization of the two larger complexes preserves the structural motif seen in complex **3**, the Au atoms of the central fragment retaining the planar arrangement between the two planes of Cu(I) ions.

According to the theoretical calculations, the Au−Au bond distances between the central fragment and the "belt" increase as a function of the size of the complex. In dication **3** and trication **1**, the Au−Au bond lengths between the central fragment and the "belt" are all equal (2.89 and 3.06 Å, respectively), while in the largest pentacation, **6**, the three supramolecular Au−Au bond lengths are 3.11, 3.46, and 3.91 Å. The increasing distance between the central fragment and the "belt" can be partially attributed to electrostatic repulsion rising between the two fragments. The respective formal charges of the central part in the dicationic, tricationic, and pentacationic complexes are −1, 0, and +2, while the "belt" fragment has a +3 formal charge in all three complexes. This gives rise to a considerable electrostatic repulsion in the case of pentacationic complex **6**. Furthermore, it appears that the match between the diameters of the central and the "belt" fragments might not be as good for the two larger complexes as it is in the case of the smallest complex, **3**, resulting in longer Au−Au bond contacts between the central fragment and the "belt". In practice, the central part is likely to fluctuate inside the "belt" fragment, the theoretically obtained geometry representing one possible conformation of the supramolecular Au−Au bond contacts. The NMR data discussed above point to D_{3h} symmetry of the molecule in solution that represents the averaging of these conformations.

Determining the intermolecular interaction energy between the central and the "belt" fragments of the studied Au(I)−Cu(I) complexes allows investigation of the driving forces behind their supramolecular assembly. The interaction between the central fragment and the "belt" is mainly determined by the electrostatic and dispersion interactions between the fragments. Because the dispersion interactions such as the aurophilic Au−Au attraction are not properly accounted for at the DFT level of theory,[40] the magnitude of the intramolecular interaction energies was investigated using the electron-correlated SCS-MP2 method. In the case of dicationic complex **3** having favorable electrostatic attraction between the central and the "belt" fragments and the shortest supramolecular Au−Au bond contacts, the interaction energy between the central and "belt" fragments is 1040 kJ/mol. As the size of the supramolecular complex increases, the supramolecular Au−Au bond contacts become longer, decreasing the significance of the attractive Au−Au interactions. For the larger tricationic and pentacationic complexes, the interaction energy between the central and the "belt" fragments is 690 and 130 kJ/mol, respectively. The energetic trend observed for the three complexes illustrates how the supramolecular assembly becomes less favorable as the formal charge of the central fragment changes from −1 to +2. Considering the electrostatic interactions between the fragments, the "layered" charge distribution of the central fragment is likely have a stabilizing effect on the supramolecular complexes. The $[PhC_2AuC_2Ph]$ rods with a formal −1 charge form the outermost "layer" of the central fragment, being in the closest contact with the positively charged "belt" fragment. While the calculations neglect the effect of counterions and solvent molecules, they reproduce the stability trends observed experimentally. For example, **3** is almost infinitely stable in solution in the absence of water and acidic admixtures, whereas **1** and **6** slowly decompose in a solution of acetone, dichloromethane, or chloroform. In the latter case, decomposition is faster due to evidently acidic admixtures formed in these solvents under exposure to light. The effect of light is particularly visible in photophysical experiments under laser irradiation. Quantum yields of luminescence for these complexes were determined under steady-state (3−10 s) laser irradiation, and no decomposition of **3** was detected during the experiments. In the case of bigger congeners, a nearly immediate drop in luminescence intensity was observed. Overall, while the aurophilic and other dispersion interactions have an effect on the assembly of the supramolecular Au(I)−Cu(I) complexes, the electrostatic interactions are likely to play the most significant role in their chemistry.

Characterization of the frontier orbitals of the "rods-in-belt" complexes at the DFT level of theory facilitates the analysis of their electronic structure and photophysical properties. The frontier molecular orbitals of dicationic

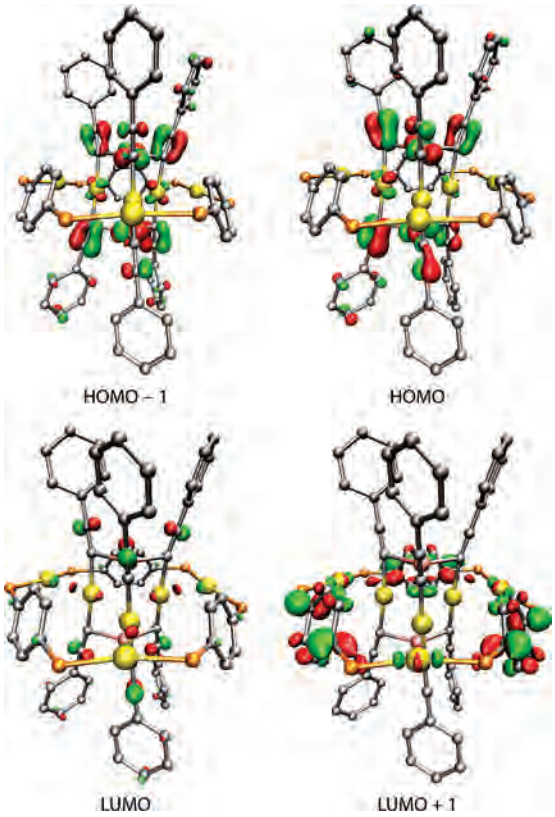

Figure 10. Selected frontier molecular orbital isodensity plots for the dicationic Au(I)−Cu(I) complex **3** (isodensity value 0.04). Phenyl rings of the "belt" fragment and hydrogen atoms omitted for clarity.

complex **3** are illustrated in Figure 10. The HOMO and HOMO − 1 of complex **3** are delocalized over the whole central fragment, with the most significant contributions coming from d(Cu), d(Au), and π(C≡C) orbitals. The main contributions to LUMO come from central fragment sp(Au), sp(Cu), and π*(C≡CPh) orbitals, with small contributions from the "belt" fragment. LUMO + 1 is delocalized over the "belt" fragment, with the largest contributions coming from the bridging Ph groups. The suggested frontier orbital characteristics for complex **3** are in good agreement with the characteristics determined by Yip et al. for the closely related $[Au_3Cu_2(C{\equiv}CC_6H_4Me\text{-}p)_6]^-$ complex.[66]

In the case of the larger tri- and pentacations, the composition of the HOMOs is very similar to that of dicationic complex **3**, but the LUMOs differ from those of the dicationic compound. Unlike in **3**, the "belt" fragment does not contribute to the LUMOs in the larger complexes. The larger number of Cu(I) ions in the tri- and pentacationic species results in increased mixing of the nonbonding sp(Cu) orbitals into LUMOs. This is likely to have a stabilizing effect on the LUMOs of the larger complexes, narrowing the HOMO−LUMO gap especially for the pentacationic species. The HOMO−LUMO gaps of the di-, tri-, and pentacationic complexes are 1.80, 1.72, and 1.22 eV, respectively. The calculated trend of the HOMO−LUMO gaps is in agreement with the experimentally observed behavior of the luminescence maxima of the different sized complexes. The di- and tricationic complexes with very small differences in the HOMO−LUMO gap have their luminescence maxima centered at 593 and 591 nm, respectively, while in the case of the pentacationic complex with an about 0.5 eV smaller HOMO−LUMO gap, the luminescence maximum is red-shifted to 658 nm. Comparing the determined frontier orbital characteristics to the experimental photophysical data suggests that the observed long-wavelength luminescence bands are associated with metal-centered transitions within the heterometallic Au−Cu core. Considering the effective intersystem crossing behavior indicated by the photophysical measurements, the initial excited states can also be ligand-related states such as MLCT [d(Au,Cu) → π*(C≡CPh)], but the observed long-wavelength triplet emission originates from the transition from metal sp orbitals to metal d orbitals.

Overall, the theoretical results obtained for the supramolecular Au(I)−Cu(I) complexes are in good agreement with the experimental data, supporting the proposed "rods-in-belt" structural motif. Theoretical studies also suggest that the observed efficient long-wavelength luminescence originates from metal-centered transitions within the heterometallic Au−Cu core.

Conclusion

The results presented here show that self-assembling of relatively simple alkynyl−diphosphine complexes of Au(I) and Cu^+ ions affords supramolecular "rods-in-belt" aggregates. The $[PhC_2AuC_2Ph]^-$ "rods" are held together by Cu−Au, π−C≡C−Cu, and Au−Au bonding to form central heterometallic clusters, which are "wrapped" about by the $[Au_3(PP)_3]^{3+}$ "belts", anchored to the central part by Au−Au bonds. The complexes obtained display very similar structural patterns, the particular composition of which is determined by the size of the oligophenylene backbone of the diphosphine and may be described by a general formula $[\{Au_xCu_y(C_2Ph)_{2x}\}Au_3\{PPh_2{-}(C_6H_4)_n{-}PPh_2\}_3]^{3+(y-x)}$ (n = 1, 2, 3; $x = (n + 1)(n + 2)/2$; $y = n(n + 1)$). These complexes demonstrate extremely efficient luminescence with a maximum quantum yield of 0.92, comparable with that of well-known organic dyes. However, it was experimentally demonstrated that an increase of the size of the aggregates leads to a decrease in photostability and photoefficiency that was confirmed by computational studies. The interaction between the central part and the tricationic "belt" is mainly determined by the electrostatic and dispersion interactions; thus, the supramolecular assembly becomes less favorable due to the appearance of electrostatic repulsion as the formal charge of the central fragment changes from −1 to +2. The most interesting feature of this chemistry is a universal character of self-assembling; moreover, analogous

(62) Müller, T. E.; Choi, S. W.-K.; Mingos, D. M. P.; Murphy, D.; Williams, D. J.; Yam, V. W.-W. *J. Organomet. Chem.* **1994**, *484*, 209–224.
(63) Li, D.; Hong, X.; Che, C.-M.; Lo, W.-C.; Peng, S.-M. *J. Chem. Soc., Dalton Trans.* **1993**, 2929–2931.
(64) Wong, K. M.-C.; Hung, L.-L.; Lam, W. H.; Zhu, N.; Yam, V. W.-W. *J. Am. Chem. Soc.* **2007**, *129*, 4350–4365.
(65) Huang, C.-C.; Lin, Y.-C.; Lin, P.-Y.; Chen, Y.-J. *Eur. J. Org. Chem.* **2006**, 4510–4518.
(66) Yip, S.-K.; Chan, C.-L.; Lam, W. H.; Cheung, K.-K.; Yam, V. W.-W. *Photochem. Photobiol. Sci.* **2007**, *6*, 365–371.

reactions involving functionalized phenylacetylenes or Au(I) and Ag(I) precursors give very similar heterometallic aggregates, the characterization of which and study of their photophysical properties are now in progress.

Acknowledgment. Financial support from the Academy of Finland (I.O.K.) and Russian Foundation for Basic Research (Grant 07-03-00908-a) is acknowledged.

Supporting Information Available: X-ray crystallographic data in CIF for **3**; $^{1}H-^{1}H$ COSY spectra of **3** and **6**; $^{1}H-^{13}C$ HSQC spectrum of **6**; ESI-mass spectrum of **3**; natural population analysis, optimized Cartesian coordinates, and absolute energies of the studied systems in atomic units. This material is available free of charge via the Internet at http://pubs.acs.org.

IC801073K